ADVANCED ELECTRONIC MATERIALS Open Access
www.advelectronicmat.de

Observation of Mobility Above 2000 $cm^2/V\ s$ in 2DEG at $LaInO_3/BaSnO_3$ Interface by Electric-Double-Layer Gating

*Jaehyeok Lee, Hyeongmin Cho, Jisung Park, Bongju Kim, Darrell G. Schlom, and Kookrin Char**

The $LaInO_3/BaSnO_3$ heterostructure has recently emerged as a promising platform for realizing 2D electron gas (2DEG) with unique transport properties, including excellent field-effect at room temperature. However, there is a limit to improving its mobility due to intrinsic defects including the threading dislocations occurring during film growth. In spite of such high density defects at present, as an effort to increase the mobility of the 2DEG, the 2D carrier density to 10^{14} cm^{-2} by ionic-liquid gating is increased and we found the resulting 2DEG mobility enhancement up to 2100 $cm^2\ V^{-1}\ s^{-1}$ at 10 K, which is consistent with the fact that 2-dimensionality offers more effective screening for defects. This findings offer insights into the properties of 2DEG formed with perovskite oxide semiconductor $BaSnO_3$ as well as highlight its future potential for applications.

1. Introduction

For decades, research on 2DEG has been carried out in a variety of material systems owing to their high electron mobility transistor (HEMT) device applications[1,2] and intriguing quantum phenomena.[3–5] These are well-known conventional 2DEG heterostructures, such as AlGaAs/GaAs,[1,6,7] AlGaN/GaN,[2,8–10] and MgZnO/ZnO heterostructures,[11–14] where 2D carrier density (n_{2D}) is reported to be $\approx 10^{11}$ cm^{-2} at AlGaAs/GaAs interface and to be $\approx 10^{13}$ cm^{-2} at AlGaN/GaN and MgZnO/ZnO interfaces, and the electron mobility (μ) has increased up to more than 10^6 $cm^2\ V^{-1}\ s^{-1}$ as the defect density decreases along with the progress of the fabrication process. In the case of the AlGaAs/GaAs System, Si dopants are intentionally doped into the AlGaAs layer, which is called modulation doping, and they are ionized by band bending near the interface and the resulting free electrons are transferred to the quantum well formed in the GaAs layer. The quantum well is formed at the interface due to the conduction band offset (CBO) between GaAs and AlGaAs.[6,7] In the case of the AlGaN/GaN and MgZnO/ZnO systems, on the other hand, deeper quantum wells form from the sum of CBO and polarization discontinuity, which is due to the generation of piezoelectric polarization in strained AlGaN and MgZnO at each interface in addition to the spontaneous polarization discontinuity.[8–14] In these heterostructures, the unintentional donors act as dopants. The unintended donors in the larger band-gap material layer come from vacancies or impurities such as N vacancies or O impurities in AlGaN, and O vacancies in MgZnO.

Like the conventional heterostructures in which a quantum well is formed at the interface by CBO and polarization discontinuity, it has been reported that 2DEG is also formed at the polar/non-polar interface of two perovskite oxides, $BaSnO_3$ (BSO) and $LaInO_3$ (LIO).[15–22] BSO is a cubic perovskite with a wide band gap of 3.1 eV and has a bulk lattice constant of 4.116 Å.[23] This material is easily doped with n-type dopants such as La dopant,[24,25] and has high carrier density ($n_{3D} \sim 10^{20}$ cm^{-3}) and high electron mobility ($\mu \sim 300$ $cm^2\ V^{-1}\ s^{-1}$) as well as high oxygen stability.[26–29] LIO is an orthorhombic perovskite of a $GdFeO_3$-type[30] with a wide band gap of 5.0 eV[31] and its pseudocubic lattice constant (a_{pc}) is calculated as 4.117 Å, which is almost matched to the lattice constant of BSO.[32,33] When depositing the $LaInO_3/BaSnO_3$ (LIO/BSO) double layers on $SrTiO_3$, $NdScO_3$, and MgO substrates, sheet conductance enhancement by four or five orders of magnitudes, compared to that of a single BSO layer, was observed even at room temperature.[15–17,22] It was experimentally derived that the CBO between the two materials is $\approx$1.6 eV,[31] but since both the cubic BSO and the orthorhombic LIO are centrosymmetric, these materials cannot have spontaneous polarization in the bulk state and it is difficult to introduce the concept of polarization discontinuity described in conventional 2DEGs. Nevertheless, to explain the conductance enhancement of the LIO/BSO interface, a newly defined "interface polarization" model was introduced, in which polarization

J. Lee, H. Cho, B. Kim, K. Char
Institute of Applied Physics
Department of Physics and Astronomy
Seoul National University
Seoul 08826, South Korea
E-mail: kchar@snu.ac.kr

J. Park, D. G. Schlom
Department of Materials Science and Engineering
Cornell University
Ithaca, New York 14853, USA

The ORCID identification number(s) for the author(s) of this article can be found under https://doi.org/10.1002/aelm.202400811

DOI: 10.1002/aelm.202400811

in polar orthorhombic LIO exists only in the four unit cells near the interface with cubic BSO.[17,20] Inversion symmetry breaking at the orthorhombic/cubic interface would cause polar perovskite LIO to possess polarization near the symmetry-broken interface, which shows up experimentally as the peak in the specific sheet conductance and n_{2D} of the heterostructures when measured as a function of LIO thickness.[17] Furthermore, the energy band structure and the corresponding quantum well at the interface in the "interface polarization" model were calculated using the self-consistent Poisson−Schrödinger (P−S) formalism simulations.[20] In the simulation, the confinement length of the quantum well was calculated to be ≈1 to 2 nm, and the following previous experimental results prove that the carriers are indeed confined to the 2-dimension: thermopower measurement[20] and capacitance–voltage (C–V) profiling[22] of the LIO/BSO heterostructures.

These 2D carriers are generally expected to have higher mobility than those of the BSO film because high carrier density can be obtained without dopants which act as a scattering source. However, the mobility of BSO-based 2DEG reported so far has not exceeded 100 cm^2 V^{-1} s^{-1}.[15–17,34] Defects within BSO including threading dislocations, other cation vacancies and anti-site defects significantly limit the ultimate mobility of this system.[35–37] Additionally, any BaO-InO_2 interface termination, different from the ideal SnO_2-LaO, will generate local potential variations, also resulting in extra scattering.[21,38] Various methods have been attempted to reduce such defects and enhance mobility, including the development of high-quality crystal growth techniques, optimization of synthesis conditions to minimize defect formation,[27,39–42] optimization of substrates and buffer layers,[43–46] and active control of the interface termination layer.[21,38] Alternatively, one way to increase mobility that can be combined with structural improvements is to modulate carrier density to a higher level.[47] As the carrier density increases, the charged defects become better screened, diminishing the resistance felt by electrons and thereby enhancing mobility.

Ionic-liquid (IL) gating is one of the methods to modulate high carrier density.[48–52] Ionic-liquid gating uses a liquid which contains ions as a gate, unlike conventional field effect transistors that use solid gates. When a gate bias is applied to the gate pad in the liquid, an electric-double-layer (EDL) is created on the surface of the film and modulates the carrier of the film. Using such liquid gating, a strong electric field can be applied to an area of 1 nm or less, enabling high carrier density modulation exceeding 10^{14} cm^{-2}.[48] However, this method presents a problem where the ionic gate and material can react chemically and physically at the surface, potentially creating defects such as oxygen vacancies,[48] especially at high bias. These newly formed defects can act as scattering sources for the modulated carriers, thereby causing a reduction in mobility. Fortunately, 2DEGs are relatively free from this issue compared to single-layer films. This is because the region where carriers accumulate and flow is away from the surface where such interaction can take place. Defects formed on the surface do not directly disrupt the flow of electrons. Ironically, while oxygen vacancies and similar defects near the oxide surface leave scattering sources at the surface, they can also act as donors in LIO, facilitating the transfer of carriers into the 2DEG at the surface of BSO and enabling higher mobility.[53]

In this work, to achieve high mobility, we modulated a 2DEG based on MBE-grown BSO with reduced defects using EDL. This enabled us to achieve a mobility exceeding 2000 cm^2 V^{-1} s^{-1} at 10 K, which is a level previously unreported in BSO systems. Such large improvement in mobility suggests that 2DEG at the LIO/BSO interface could be suitable for various applications, such as HEMTs, and also indicates the potential for observing diverse quantum phenomena.[3–5]

2. Results and Discussions

2.1. Ionic-Liquid Gating

The heterostructural LIO/BSO samples were fabricated into Hall-bar geometry through photolithography and Ar-ion milling. The fabrication process is shown in **Figure 1a** detailed description is provided in the methods section following the conclusion. In order to construct the LIO/BSO using electric-double-layer, the following steps were added to the Hall-bar patterned LIO/BSO sample: First, an additional Au wire as a gate electrode to apply the gate voltage (V_{GS}) was placed directly above the channel region with a gap of ≈1 mm. Second, a drop of ionic-liquid (IL) was dropped on the sample immediately before loading it into the PPMS (Physical Property Measurement System) to minimize water contamination. Before use, the IL was baked in a hot plate at 110 °C for 12 h to remove moisture. The liquid used in these experiments was diethylmethyl ammonium bis(trifluoromethylsulfonyl)imide, which is also known as $[DEME]^+[TFSI]^-$. When a positive V_{GS} is applied, anions of the IL move toward the gate electrode and accumulate while cations of the IL move toward the surface of the sample and accumulate. Then, charges are balanced by accumulation of electrons on the side of the interface between the sample and the $[DEME]^+$, forming an electric-double-layer.

Figure 2a shows a schematic of the Hall-bar patterned LIO/BSO sample with gate electrode and IL. Before carrying out full-scale temperature- and gate voltage-dependent transport experiments, some basic tests were performed to demonstrate the feasibility of gating using IL. The sheet resistance (R_s) of the channel and the leakage current (I_{GS}) between the channel and the gate electrode were tested when the V_{GS} was applied. When the V_{GS} was applied at 220 K (above the freezing temperature of 180—190 K) we held it for 20 min before measurement in order to stabilize IL and give enough time for $[DEME]^+$ and $[TFSI]^-$ in the liquid to align.[52] Figure 2b shows change of R_s and I_{GS} as a function of V_{GS} at 220 K, where V_{GS} was swept from 0 to 8 to 0 V at 2 V intervals, and a time interval of 20 min was set per voltage. It is confirmed that the R_s of the sample decreases as the applied V_{GS} increases, and the R_s increases with a similar slope as the applied V_{GS} decreases. We also confirmed, after sufficient time at 0 V on returning, that R_s is almost reversible to the prebias R_s. The I_{GS} maintains less than 2 μA up to 8 V, which is a negligibly small value compared to drain-source current (I_{DS}) of 10 μA. Based on these tests, the feasibility of IL could be demon-

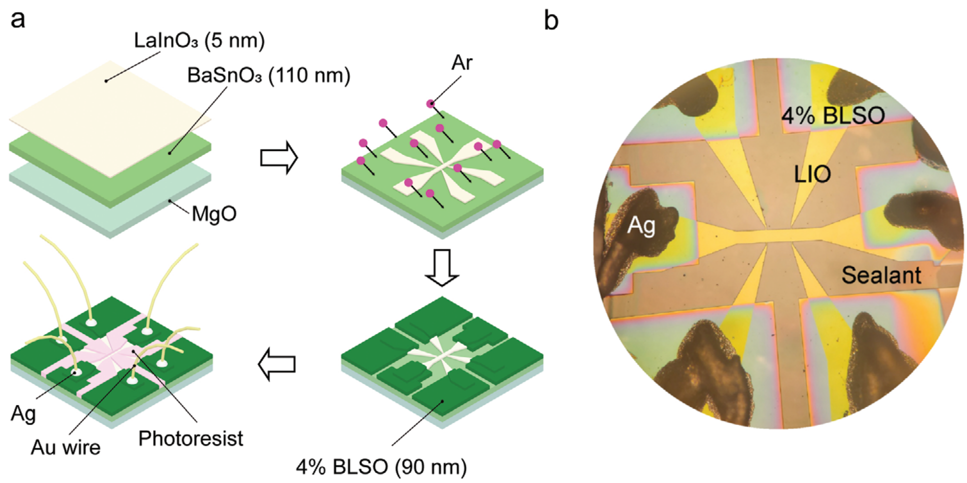

Figure 1. a) Fabrication process of Hall-bar pattern. BSO is deposited using MBE, followed by the deposition of LIO using PLD. Hall-bar geometry is fabricated through ion milling. Contact pads of 4% BLSO are deposited using PLD with a stencil mask. Areas not intended for modulation are covered with photoresist, and for measurements, gold wires are affixed to the pads using silver paste. b) A top view image of the finished sample with a Hall-bar geometry and 4% BLSO pads, as seen through an optical microscope.

strated, and temperature- and gate voltage-dependent transport experiments of the LIO/BSO sample were then carried out.

2.2. Electrical Properties Under Electric Field

To investigate the effect on the carrier density (n_{2D}) and electron mobility (μ) by ionic-liquid gating, the transport properties were measured while varying the gating bias and temperature. **Figure 3a** shows temperature- and gate voltage-dependent transport properties of the sample, where the specific resistance R_s is plotted as a function of T at different V_{GS} (0 to 8 V at intervals of 1 V). Each V_{GS} was applied at 220 K and kept for 20 min for $[DEME]^+$ and $[TFSI]^-$ ions in the liquid to align and settle. Subsequently, after cooling the sample to 2 K while keeping the V_{GS} constant, all measurements were performed as we raised the temperature. Considering the instability of E-field applied IL around room temperature, the range of temperature during measurements was set from 2 to 220 K. Each change of bias voltage of V_{GS} was applied at 220 K. The anomalies observed in R_s within the temperature range from 150 to 220 K are observed in other IL gating.[48] The R_s decreases as V_{GS} increases, showing a decrease by 3 orders of magnitude at 8 V from the 0 V value. Temperature dependence of R_s indicates that there is a transition from a semiconducting to a metallic behavior around $V_{GS} \sim 2$ V, where the corresponding R_s value is ≈10 kΩ, in agreement with the Mott's criteria for metal-insulator transition.[54] Interestingly, in the metallic regime ($V_{GS} > 2$ V) there exists a very slow and slight upturn in R_s at low temperatures almost in the shape of log T – see Figure S1 (Supporting Information). These results

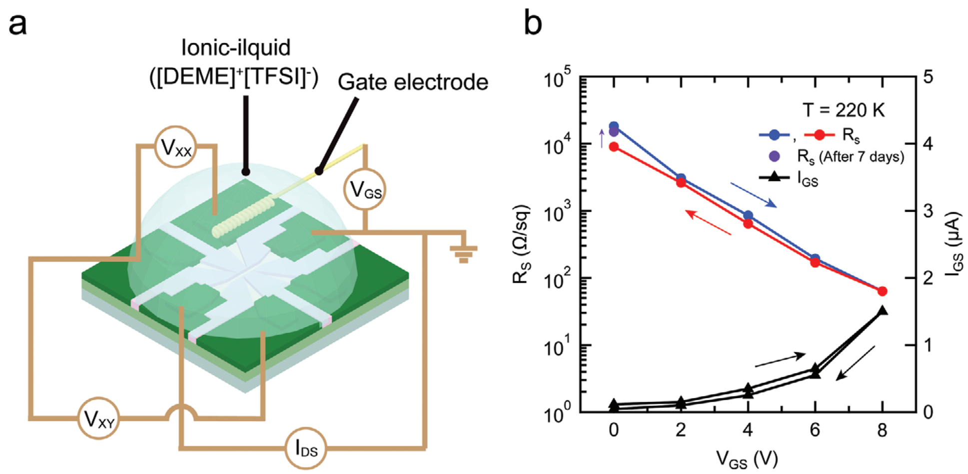

Figure 2. a) A schematic diagram with the addition of the ionic-liquid ($[DEME]^+[TFSI]^-$) for the Hall-bar patterned sample for liquid gating. A sealant to prevent gating of un-doped BSO and a gate electrode for top gating were added. b) Change of sheet resistance (R_s) and leakage current (I_{GS}) as a function of gate voltage (V_{GS}) at 220 K. V_{GS} was swept from 0 to 8 to 0 V at 2 V intervals, and at the time of application, a time interval of 20 min per voltage was set to provide enough time for $[DEME]^+$ and $[TFSI]^-$ in the ionic-liquid to align. After 7 days, the change in R_s (purple circle) was observed.

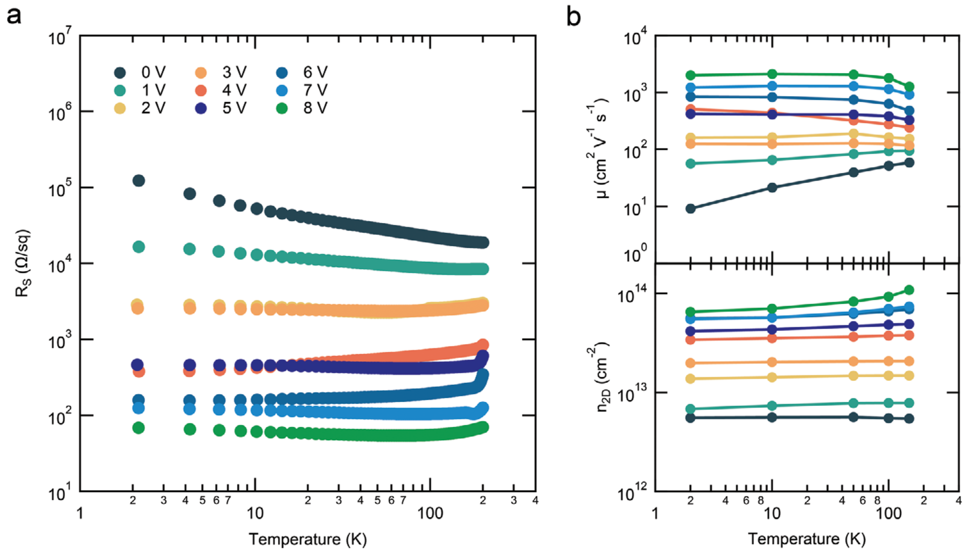

Figure 3. Temperature-dependent transport properties of LIO/BSO heterostructures. a) Change of sheet resistance (R_s), and b) electron mobility (μ) and sheet carrier density (n_{2D}) as a function of temperature (T) at different gate voltages (0 to 8 V at intervals of 1 V). As V_{GS} increases, R_s decreases, but n_{2D} continues to increase, approaching 10^{14} cm^{-2}, and μ also increases along with it, exceeding 10^3 cm^2 V^{-1} s^{-1}.

suggest that even with the increase of n_{2D} by IL gating and the corresponding increase of μ, the effects of weak localization (WL) remains visible at low temperatures. In Figure 3b n_{2D} and μ as a function of T at different V_{GS} (0 to 8 V at intervals of 1 V) are plotted. The n_{2D} was calculated by Hall measurements which remained linear up to 7 T for all the bias voltages and temperatures. (Figures S2 and S3, Supporting Information). Such linearity in our LIO/BSO 2DEG is different from the non-linearity observed for the $LaAlO_3/SrTiO_3$ (LAO/STO) interface.[55] The n_{2D} for each gate bias applied is almost temperature-independent, which is also seen in Figure S4 (Supporting Information). The slight tendency for the n_{2D} to decrease at lower temperatures at high bias, but not at lower biases, is not well understood at this point. As V_{GS} increases, n_{2D} continues to increase, and the maximum modulation of n_{2D} reaches up to ≈10^{14} cm^{-2}, which is higher by 1 order of magnitude than that modulated in conventional solid-gate FETs.[16,31,34,56,57] Furthermore, it is confirmed that μ also increases along with the increase in n_{2D}, and the value increases up to ≈2102 cm^2 V^{-1} s^{-1} at 10 K (see Figure S1, Supporting Information), which is the largest reported mobility for BSO-based systems including heterostructures to date.[15–17,21,34,50,51] This demonstrates that IL gating can be exploited effectively for 2D carrier accumulation and electron mobility enhancement in the 2D LIO/BSO system.

In particular, when the V_{GS} of 8 V was applied, a mobility value of 1999 cm^2 V^{-1} s^{-1} was recorded at a temperature of 2 K. This temperature and mobility are the conditions under which the Shubnikov-de Hass (SdH) effect can be expected to be observed.[58,59] However, our high carrier density of 6.52 × 10^{13} cm^{-2} at 2 K at 8 V gate bias (see Figure S1, Supporting Information) predicts the 193rd SdH oscillation occurring at 7 T, according to $i = n_{2D}\, h/2eB$, where i is the order of oscillation, n_{2D} is the 2D carrier density, h is the Planck constant, e is the elementary charge, and B is the magnetic field. Such high-order oscillations are difficult to observe experimentally. If we can further reduce the defects such as threading dislocations, for example by using a lattice-matched substrate,[60] and other defects, we may obtain high mobility at lower $n_{2D}$and then expect to observe the SdH oscillation in higher magnetic fields.

2.3. Relationship Between Carrier Density and Mobility

In semiconductors, carrier density and electron mobility are deeply related. There are several scattering mechanisms that limit mobility. These mechanisms include ionized-impurity, acoustic-phonon, and polar-optical phonon scattering. Depending on which mechanism becomes dominant, the relationship between them shows various trends.[61] Factors that determine the dominance of a mechanism include temperature and structure. Typically, in low-temperature environments where phonons are reduced, the limitation of mobility due to ionized-impurity scattering becomes more pronounced. In the case of mobility limitations due to defects such as ionized-impurities or dislocations, changes in mobility in response to changes in carrier density tend to be larger in 2-dimension than in 3-dimension.[47] This is because the screening effect of defects by electrons is more efficient in 2D than in 3D. Numerous experimental and theoretical studies have been conducted on how mobility in 2D structures is affected by carrier density and impurity scattering.[61–64]

Figure 4 presents a graph of μ versus n_{2D} at 150 and 10 K. This graph provides a trend line representing the relationship $\mu \propto n_{2D}^{3/2}$ to illustrate the correlation between μ and n_{2D}. The fact that carrier density and mobility have a relationship of $\mu \propto n_{2D}^{3/2}$ means that the layer has 2-dimensionality.[47] In the Figure we included data from Tohoku University for comparison with crimson triangle points, representing their data from IL gating of a 248 nm thick BSO sample, where V_{GS} ranges from 0 to 6 V at 150 K.[50] The green and blue circles are our data from the 2DEG

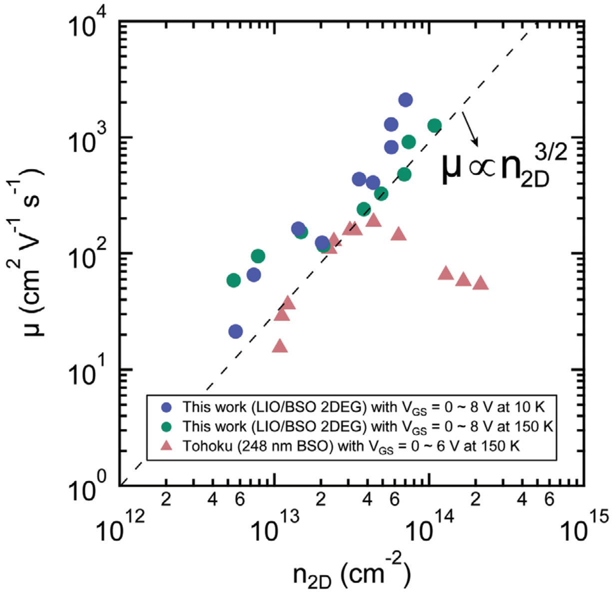

Figure 4. Mobility (μ) as a function of n_{2D} for 2DEG with gate voltage at 150 K (green circles) and 10 K (blue circles). For comparison, the data from another BSO-based system is also shown: 248 nm thick BSO film via IL gating from Fujiwara et al. at Tohoku University at 150 K (crimson triangles).[50] The dotted line represents a line for a relation of $\mu \propto n_{2D}{}^{3/2}$.

with V_{GS} applied from 0 to 8 V. In our data, when the gate V_{GS} is increased to 8 V, the n_{2D} reaches its peak at $\approx 1.08 \times 10^{14}$ cm^{-2} at 150 K. At this peak, the electron mobility also attains a value of 1262 cm^2 V^{-1} s^{-1} (see Figure S1, Supporting Information) at 150 K. Both samples follow $\mu \propto n_{2D}{}^{3/2}$ trend. However, while 2DEG maintains this trend up to 8 V, the mobility in the 248 nm BSO film by PLD does not increase beyond 4 V even as n_{2D} increases. The observation of bell-shaped μ versus n_{2D} curves suggests the existence of larger density of defects in BSO made by PLD, which sets the upper bound for high mobility value.[53,65] Additionally, the direct IL gating of a BSO film may also generate oxygen vacancies on the BSO surface at high bias, which will limit the mobility enhancement. The increasing trend of mobility up to 8 V in 2DEG is expected to decrease eventually with higher carrier density modulation due to such scattering effects as surface roughness.

2.4. Electrical Properties in Magnetic Field

In the magnetic field applied in the perpendicular direction we observed negative magnetoresistance (nMR), as shown in **Figure 5**. In Figure 5a, the gradually decreasing trend of nMR is observed with increasing gate voltage at 2 K. At the same time, in Figure 5b, nMR is confirmed to decrease with increasing temperature at zero bias voltage. These data show that our system is in a WL regime at low temperatures despite high carrier density of $\approx 10^{14}$ cm^{-2} and mobility above 10^3 cm^2 V^{-1} s^{-1}, although higher carrier density appears to reduce the effect of WL The upturn in resistance in high magnetic field above 3 T at 2 K and zero gate bias may be coming from the correlation effect due to insufficient screening, as observed for low mobility 2DEG in Si metal-oxide-semiconductor FETs.[66]

The nMR in our system is in contrast to the case of the LAO/STO heterostructures, which is not affected by WL due to low defect density in STO crystals and instead shows positive magnetoresistance (pMR) from the spin-orbit coupling (SOC) of the conducting electrons.[67,68] Additionally, STO-based systems can show MR with weak anti-localization (WAL) shape as the gating bias is applied, which is not the case for our heterostructures.[69,70] The origin for such difference can be inferred from the Sn 5s orbital characteristics of the charge carriers in BSO. In the s orbital, the angular momentum quantum number (notated as l) is 0, and the resulting spin-orbit coupling term is 0. Therefore, the SOC-dependent WAL effect is supposed to be very small in BSO-based systems even though n_{2D} is modulated to 10^{14} cm^{-2} via gating.[71]

3. Conclusion

In summary, to achieve higher mobility, we modulated 2DEG at LIO/BSO interface using MBE-grown BSO through ionic liquid gating. As the gate voltage increased, 2DEG showed accumulation of carriers, and the mobility increased by following $\mu \propto n_{2D}{}^{3/2}$. These LIO/BSO heterostructures showed the highest mobility ever reported, at 2102 cm^2 V^{-1} s^{-1} at 10 K, when the carrier density is modulated up to 7.04×10^{13} cm^{-2} at a V_{GS} of 8 V. Despite its high mobility, SdH oscillation could not be observed experimentally due to its high carried density and the resulting high oscillation order at 7 T. Nevertheless, our work confirms that the mobility of 2DEG at the interface of LIO/BSO can be further enhanced as we reduce the defects in BSO and its interfacial termination layer.

4. Experimental Section

Film Growth: All layers of the samples used in the experiment were grown epitaxially. BSO was grown on (001) MgO substrate for this study, deploying adsorption-controlled growth method on Veeco GEN10 molecular-beam epitaxy system with separate Ba and SnO_2 sources. The details of the growth method are presented elsewhere.[39] Initially, BSO was grown to a thickness of 110 nm on an MgO substrate using MBE, chosen for its lower defect density than the BSO grown by PLD, resulting in higher-mobility films.[27,39] This reduced defect density was critical for creating a 2DEG with enhanced mobility. The growth progress of BSO was tracked using reflection high-energy electron diffraction (RHEED) patterns, as shown in Figure S5 (Supporting Information). After the growth, atomic force microscopy (AFM) and X-ray diffraction (XRD) analyses confirmed that the BSO films exhibited a flat surface with 380 pm roughness and were single-phase, as demonstrated in Figure S6 (Supporting Information). Subsequently, 5 nm thick LIO was deposited on the BSO layer using PLD to form a 2DEG at the interface, with the LIO layer thickness optimized to 5 nm to balance environmental stability and high conductivity.[17] Subsequently 4% BLSO used as a contact pad was grown by PLD using a KrF excimer laser. Both LIO and BLSO layers were deposited under the same conditions: a pressure of 100 mTorr, a temperature of 750 °C, a target-sample distance of 52 mm, and a laser fluence of 1.43 J cm^2. After each deposition, the samples were cooled slowly from 750 °C to room temperature in 600–700 Torr oxygen atmosphere. The targets used for PLD deposition were all manufactured by Toshima Manufacturing Co. in Japan.

Device Fabrication: To minimize the noise during Hall measurements, a Hall-bar pattern instead of Van der Pauw geometry was employed. The 2DEG was shaped into a Hall-bar geometry using photolithography and Ar-ion milling. The fabrication process used for the samples in the measurements is illustrated in detail in Figure 1a. Following this, areas outside

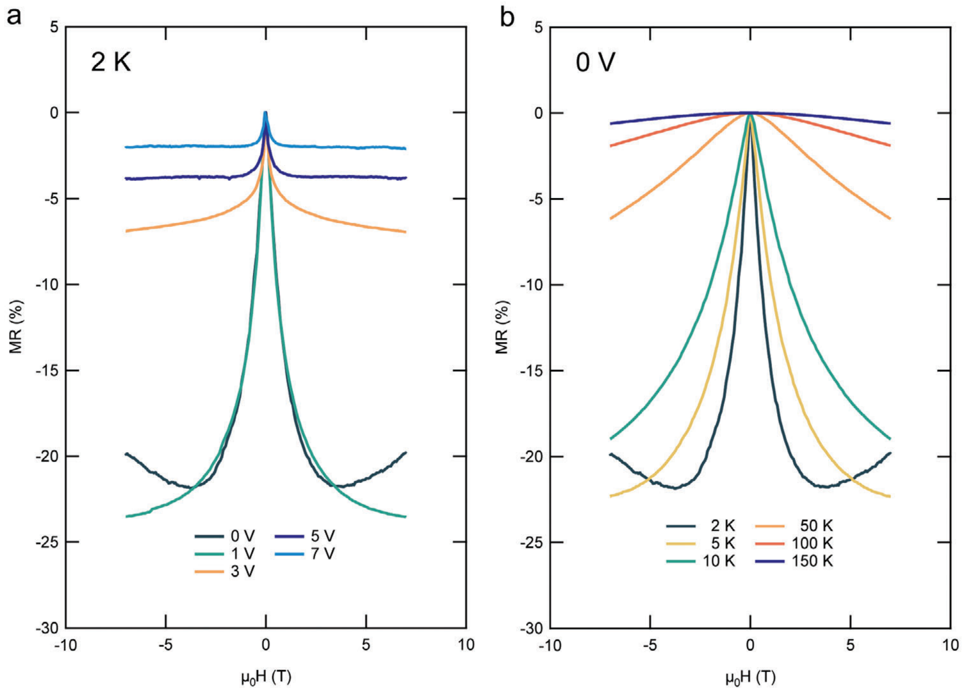

Figure 5. Changes of magnetoresistance in magnetic fields. Change of magnetoresistance a) with increasing gate voltage at 2 K, and b) with increasing temperature under 0 V.

the Hall-bar geometry were precisely etched by 40 nm using ion-milling, defining a channel with dimensions of 300 µm in length and 150 µm in width. Next, 90 nm 4% BLSO was deposited as a contact pad using PLD with a stencil mask, where 4% BLSO consistently ensures a stable ohmic contact with the BSO system.[72] Afterward, to prevent modulation in areas other than the Hall-bar channel, all areas except the Hall-bar geometry and contact pad were protected with a sealant. Photoresist, used as the sealant, was confirmed to be electrically insulating. Gold wires were subsequently attached to the contact pads using silver paste for low-temperature measurements. Figure S7 (Supporting Information) shows that 2DEG was formed on the BSO film after LIO deposition and that the formed 2DEG was maintained even after the fabrication process described above. The top view of the completed Hall-bar patterned sample with the 4% BLSO contact pads under an optical microscope was shown in Figure 1b. From the microscope, it was confirmed that the sealant covers the etched BSO surface, and the length and width of the channel were 300 and 150 µm, respectively.

Acknowledgements

J.L. and H.C. contributed equally to this work. J. Park, one of the authors, was currently with Applied Materials in Santa Clara, CA, USA. This work was supported by the National Research Foundation of Korea (NRF) grant funded by the government of Korea (MSIT) (No. 2023R1A2C100435311). Part of this study had been performed using facilities at Center for Correlated Electron Systems of Institute of Basic Science in Korea, Seoul National University. Part of this work was supported by the Research Center Program of the Institute of Basic Science in Korea (Grant No. IBS-R009-D1).

Conflict of Interest

The authors declare no conflict of interest.

Data Availability Statement

The data that support the findings of this study are available in the supplementary material of this article.

Keywords

2DEG, high mobility, ionic liquid gating, LaInO3/BaSnO3 interface, weak localization

Received: October 24, 2024
Revised: December 3, 2024
Published online:

[1] T. Mimura, S. Hiyamizu, T. Fujii, K. Nanbu, *Jpn. J. Appl. Phys.* **1980**, *19*, L225.
[2] J. P. Ibbetson, P. T. Fini, K. D. Ness, S. P. DenBaars, J. S. Speck, U. K. Mishra, *Appl. Phys. Lett.* **2000**, *77*, 250.
[3] K. v. Klitzing, G. Dorda, M. Pepper, *Phys. Rev. Lett.* **1980**, *45*, 494.
[4] K. v. Klitzing, *Rev. Mod. Phys.* **1986**, *58*, 519.
[5] D. C. Tsui, H. L. Stormer, A. C. Gossard, *Phys. Rev. Lett.* **1982**, *48*, 1559.
[6] R. Dingle, H. L. Störmer, A. C. Gossard, W. Wiegmann, *Appl. Phys. Lett.* **1978**, *33*, 665.
[7] H. L. Störmer, A. Pinczuk, A. C. Gossard, W. Wiegmann, *Appl. Phys. Lett.* **1981**, *38*, 691.
[8] R. Gaska, M. S. Shur, A. D. Bykhovski, A. O. Orlov, G. L. Snider, *Appl. Phys. Lett.* **1999**, *74*, 287.
[9] I. P. Smorchkova, C. R. Elsass, J. P. Ibbetson, R. Vetury, B. Heying, P. Fini, E. Haus, S. P. DenBaars, J. S. Speck, U. K. Mishra, *J. Appl. Phys.* **1999**, *86*, 4520.

[10] M. J. Manfra, N. G. Weimann, J. W. P. Hsu, L. N. Pfeiffer, K. W. West, S. Syed, H. L. Stormer, W. Pan, D. V. Lang, S. N. G. Chu, G. Kowach, A. M. Sergent, J. Caissie, K. M. Molvar, L. J. Mahoney, R. J. Molnar, *J. Appl. Phys.* **2002**, *92*, 338.
[11] H. Tampo, H. Shibata, K. Maejima, A. Yamada, K. Matsubara, P. Fons, S. Kashiwaya, S. Niki, Y. Chiba, T. Wakamatsu, H. Kanie, *Appl. Phys. Lett.* **2008**, *93*, 202104.
[12] H.-A. Chin, I.-C. Cheng, C.-I. Huang, Y.-R. Wu, W.-S. Lu, W.-L. Lee, J. Z. Chen, K. C. Chiu, T.-S. Lin, *J. Appl. Phys.* **2010**, *108*, 054503.
[13] A. Tsukazaki, A. Ohtomo, T. Kita, Y. Ohno, H. Ohno, M. Kawasaki, *Science* **2007**, *315*, 1388.
[14] A. Tsukazaki, S. Akasaka, K. Nakahara, Y. Ohno, H. Ohno, D. Maryenko, A. Ohtomo, M. Kawasaki, *Nat. Mater.* **2010**, *9*, 889.
[15] U. Kim, C. Park, Y. M.o Kim, J. Shin, K. Char, *APL Mater.* **2016**, *4*, 071102.
[16] Y. Kim, Y. M. Kim, J. Shin, K. Char, *APL Mater.* **2018**, *6*, 096104.
[17] Y. M. Kim, T. Markurt, Y. Kim, M. Zupancic, J. Shin, M. Albrecht, K. Char, *Sci. Rep.* **2019**, *9*, 16202.
[18] M. Zupancic, W. Aggoune, T. Markurt, Y. Kim, Y. M. Kim, K. Char, C. Draxl, M. Albrecht, *Phys. Rev. Mater.* **2020**, *4*, 123605.
[19] K. Krishnaswamy, L. Bjaalie, B. Himmetoglu, A. Janotti, L. Gordon, C. G. Van de Walle, *Appl. Phys. Lett.* **2016**, *108*, 083501.
[20] Y. Kim, S. Kim, H. Cho, Y. M. Kim, H. Ohta, K. Char, *Phys. Rev. Appl.* **2022**, *17*, 014031.
[21] S. Kim, M. Lippmaa, J. Lee, H. Cho, J. Kim, B. Kim, K. Char, *Adv. Mater. Interfaces* **2022**, *9*, 2201781.
[22] D. Pfützenreuter, S. Kim, H. Cho, O. Bierwagen, M. Zupancic, M. Albrecht, K. Char, J. Schwarzkopf, *Adv. Mater. Interfaces* **2022**, *9*, 2201279.
[23] H. J. Kim, U. Kim, T. H. Kim, J. Kim, H. M. Kim, B.-G. Jeon, W.-J. Lee, H. S. Mun, K. T. Hong, J. Yu, K. Char, K. H. Kim, *Phys. Rev. B* **2012**, *86*, 165205.
[24] S. Sallis, D. O. Scanlon, S. C. Chae, N. F. Quackenbush, D. A. Fischer, J. C. Woicik, J.-H. Guo, S. W. Cheong, L. F. J. Piper, *Appl. Phys. Lett.* **2013**, *103*, 042105.
[25] Z. Lebens-Higgins, D. O. Scanlon, H. Paik, S. Sallis, Y. Nie, M. Uchida, N. F. Quackenbush, M. J. Wahila, G. E. Sterbinsky, D. A. Arena, J. C. Woicik, D. G. Schlom, L. F. J. Piper, *Phys. Rev. Lett.* **2016**, *116*, 027602.
[26] H. J. Kim, U. Kim, H. M. Kim, T. H. Kim, H. S. Mun, B.-G.u Jeon, K. T. Hong, W.-J. Lee, C. Ju, K. H. Kim, K. Char, *Appl. Phys. Express* **2012**, *5*, 061102.
[27] S. Raghavan, T. Schumann, H. Kim, J. Y. Zhang, T. A. Cain, S. Stemmer, *APL Mater.* **2016**, *4*, 016106.
[28] A. Prakash, P. Xu, A. Faghaninia, S. Shukla, J. W. Ager III, C. S. Lo, B. Jalan, *Nat. Commun.* **2017**, *8*, 15167.
[29] J. Shin, Y. M. Kim, Y. Kim, C. Park, K. Char, *Appl. Phys. Lett.* **2016**, *109*, 262102.
[30] S. Geller, *J. Chem. Phys.* **1956**, *24*, 1236.
[31] U. Kim, C. Park, T. Ha, Y. M. Kim, N. Kim, C. Ju, J. Park, J. Yu, J. H. Kim, K. Char, *APL Mater.* **2015**, *3*, 036101.
[32] R. Ubic, G. Subodh, *J. Alloys Compd.* **2009**, *488*, 374.
[33] H. M. Park, H. J. Lee, S. H. Park, H. I. Yoo, *Acta Crystallogr., Sect. C: Cryst. Struct. Commun.* **2003**, *59*, i131.
[34] H. Cho, D. Song, Y. Kim, B. Kim, K. Char, *ACS Appl. Electron. Mater.* **2021**, *4*, 356.
[35] H. Mun, U. Kim, H. M. Kim, C. Park, T. H. K. H. J. Kim, K. H. Kim, K. Char, *Appl. Phys. Lett.* **2013**, *102*, 252105 .
[36] H. Yun, M. Topsakal, A. Prakash, B. Jalan, J. Seok Jeong, T. Birol, K. Andre Mkhoyan, *Sci. Adv.* **2021**, *7*, eabd4449.
[37] J. Kang, J. H. Lee, H.-K. Lee, K.-T. Kim, J. H. Kim, M.-J. Maeng, J.-A.m Hong, Y. Park, K. H. Kim, *Materials* **2022**, *15*, 2417.
[38] S. Kim, B. Kim, K. Char, *APL Mater.* **2023**, *11*, 121105.
[39] H. Paik, Z. Chen, E. Lochocki, A. S. H., A. Verma, N. Tanen, J. Park, M. Uchida, S. L. Shang, B.-C. Zhou, M. Brutzam, R. Uecker, Z.-K. Liu, D. Jena, K. M. Shen, D. A. Muller, D. G. Schlom, *APL Mater.* **2017**, *5*, 116107.
[40] A. V. Sanchela, M. Wei, H. Zensyo, B. Feng, J. Lee, G. Kim, H. Jeen, Y. Ikuhara, H. Ohta, *Appl. Phys. Lett.* **2018**, *112*, 232102.
[41] W. M. Postiglione, K. Ganguly, H. Yun, J. S. Jeong, A. Jacobson, L. Borgeson, B. Jalan, K. Andre Mkhoyan, C. Leighton, *Phys. Rev. Mater.* **2021**, *5*, 044604.
[42] A. V. Sanchela, M. Wei, J. Lee, G. Kim, H. Jeen, B. Feng, Y. Ikuhara, H. J. Choab, H. Ohta, *J. Mater. Chem. C* **2019**, *7*, 5797.
[43] P. Ngabonziza, J. Park, W. Sigle, P. A. van Aken, J. Mannhart, D. G. Schlom, *Appl. Phys. Lett.* **2023**, *122*, 241902.
[44] J. Shiogai, K. Nishihara, K. Sato, A. Tsukazaki, *AIP Adv.* **2016**, *6*, 065305.
[45] H. Yun, K. Ganguly, W. Postiglione, B. Jalan, C. Leighton, K. Andre Mkhoyan, J. S. Jeong, *Sci. Rep.* **2018**, *8*, 10245.
[46] A. P. N. Tchiomo, W. Braun, B. P. Doyle, W. Sigle, P. Aken, J. Mannhart, P. Ngabonziza, *APL Mater.* **2019**, *7*, 041119.
[47] D. Jena, A. C. Gossard, U. K. Mishra, *Appl. Phys. Lett.* **2000**, *76*, 1707.
[48] S. Z. Bisri, S. Shimizu, M. Nakano, Y. Iwasa, *Adv. Mater.* **2017**, *29*, 1607054.
[49] S. Zeng, W. Lü, Z. Huang, Z. Liu, K. Han, K. G. C. Li, R. Guo, W. Zhou, H. H. Ma, L. Jian, T. Venkatesan, *ACS Nano* **2016**, *10*, 4532.
[50] K. Fujiwara, K. Nishihara, J. Shiogai, A. Tsukazaki, *Appl. Phys. Lett.* **2017**, *110*, 203503.
[51] H. Wang, J. Walter, K. Ganguly, B. Yu, G. Yu, Z. Zhang, H. Zhou, H. Fu, M. Greven, C. Leighton, *Phys. Rev. Mater.* **2019**, *3*, 075001.
[52] D. Kim, Y. Kim, B. Sohn, M. Kim, B. Kim, T. W. Noh, C. Kim, *Adv. Mater.* **2023**, *35*, 2207188.
[53] Y. Kozuka, M. Kim, H. Ohta, Y. Hikita, C. Bell, H. Y. Hwang, *Appl. Phys. Lett.* **2010**, *97*, 222115.
[54] N. F. Mott, *Metal Insulator Transition*, Taylor and Frances, London, **1974**.
[55] A. Joshua, S. Pecker, J. Ruhman, E. Altman, S. Ilani, *Nat. Commun.* **2012**, *3*, 1129.
[56] Y. M. Kim, C. Park, U. Kim, C. Ju, K. Char, *Appl. Phys. Express* **2016**, *9*, 011201.
[57] Y. M. Kim, C. Park, T. Ha, U. Kim, N. Kim, J. Shin, Y. Kim, J. Yu, J. H. Kim, K. Char, *APL Mater.* **2017**, *5*, 016104.
[58] M. Ben Shalom, A. Ron, A. Palevski, Y. Dagan, *Phys. Rev. Lett.* **2010**, *105*, 206401.
[59] A. D. Caviglia, S. Gariglio, C. Cancellieri, B. Sacépé, A. Fête, N. Reyren, M. Gabay, A. F. Morpurgo, J.-M. Triscone, *Phys. Rev. Lett.* **2010**, *105*, 236802.
[60] D. Pfützenreuter, M. Zupancic, Z. Galazka, R. Schewski, A. Dittmar, K. Irmscher, M. Albrecht, J. Schwarzkopf, *Nanotechnology* **2021**, *32*, 505609.
[61] K. Hirakawa, H. Sakaki, *Phys. Rev. B* **1986**, *33*, 8291.
[62] S. B. Lisesivdin, A. Yildiz, N. Balkan, M. Kasap, S. Ozcelik, E. Ozbay, *J. Appl. Phys.* **2010**, *108*, 013712.
[63] S. D. Sarma, E. H. Hwang, *Phys. Rev. B* **2014**, *90*, 035425.
[64] T. Ando, A. B. Fowler, F. Stern, *Rev. Mod. Phys.* **1982**, *54*, 437.
[65] J. Falson, Y. Kozuka, M. Uchida, J. H. Smet, A. T. Taka-hisaArima, M. Kawasaki, *Sci. Rep.* **2016**, *6*, 26598.
[66] D. J. Bishop, R. C. Dynes, D. C. Tsui, *Phys. Rev. B* **1982**, *26*, 773.
[67] F. J. Wong, R. V. Chopdekar, Y. Suzuki, *Phys. Rev. B* **2010**, *82*, 165413.
[68] T. Hernandez, C. W. Bark, D. A. Felker, C. B. Eom, M. S. Rzchowski, *Phys. Rev. B* **2012**, *85*, 161407(R).
[69] G. Jnawali, M. Huang, J.-F. Hsu, H. Lee, J.-W. Lee, P. Irvin, C.-B. Eom, B. D'Urso, J. Levy, *Adv. Mater.* **2017**, *29*, 1603488.
[70] A. D. Caviglia, M. Gabay, S. Gariglio, N. Reyren, C. Cancellieri, J.-M. Triscone, *Phys. Rev. Lett.* **2010**, *104*, 126803.
[71] H. Cho, Ph. D. dissertation, Seoul National University **2023**.
[72] J. Lee, H. Cho, B. Kim, M. Jeong, K. Lee, K. Char, *Appl. Phys. Lett.* **2022**, *121*, 142102.